Effect of S6 Tail Mutations on Charge Movement in *Shaker* Potassium Channels

Shinghua Ding and Richard Horn
Department of Physiology, Institute of Hyperexcitability, Jefferson Medical College, Philadelphia, Pennsylvania 19107

ABSTRACT The cytoplasmic ends of the four S6 transmembrane segments of voltage-gated potassium channels converge in a bundle crossing that acts as the activation gate that opens in response to a depolarization. To explore whether the cytoplasmic extension of the S6 segment (the S6 tail) plays a role in coupling voltage sensor and activation gate movements, we examined the effect of cysteine substitution from residues N482 to T489 on the kinetics and voltage-dependence of S4 charge movement and on the kinetics of deactivation of ionic current. Among these mutants, F484C has the steepest voltage-dependent charge movement, the largest Q–V shift, and the fastest OFF gating currents. Further study of the residue at position 484, using mutagenesis and modification of F484C by cysteine reagents, suggests that aromaticity at this position is essential to maintain normal coupling. We used periodicity analysis to appraise the possibility that the S6 tail has an α-helical structure. Although we obtained an α-periodicity index of 2.41 for gating current parameters, a new randomization test produced an indecisive conclusion about the secondary structure of this region. Taken together, our results suggest that the tail end of S6 plays an important role in coupling between activation gating and charge movement.

INTRODUCTION

Voltage-gated ion channels open and close in response to changes of membrane potential. These ion channels are composed of three interacting functional units: a selective permeation pathway (i.e., pore), gates (including activation and inactivation gates) that control access of permeant ions to the pore, and voltage sensors that move in response to changes of membrane potential (Bezanilla, 2000; Horn, 2000; Sigworth, 1994; Yellen, 1998). We have reasonable candidates for the regions of the channels that subserve these three functions, based on extensive studies, chiefly using mutagenesis and chimeric swapping, and also on the elucidation of the crystal structure of the bacterial potassium channel KcsA (Doyle et al., 1998). Voltage-gated potassium channels, for example, are formed of four subunits, each having six transmembrane segments, S1–S6. The main voltage sensors for this superfamily of ion channels are the four positively charged S4 segments. The four subunits are arranged radially around the pore, which is mainly lined by hydrophobic S6 segments, with selectivity determined by the narrow 'selectivity filter' of the extracellular S5–S6 linker (the P-loop). State-dependent modification of cysteine mutants in S6 segments of *Shaker* potassium channels suggests that the activation gate is located at the cytoplasmic ends of the S6 segments, all four of which converge in a right-handed bundle crossing (Del Camino et al., 2000; Del Camino and Yellen, 2001; Holmgren et al., 1998; Liu et al., 1997).

Extensive data show that S4 segments move in response to changes of membrane potential (Bezanilla, 2000; Horn, 2000; Sigworth, 1994; Yellen, 1998). However, the mechanisms that underlie the coupling between S4 and activation gate movements are unknown. Two hypotheses predominate (see Discussion in Horn, 2000). The first is that S4 movement pulls or twists the cytoplasmic S4–S5 linker, and that this linker is coupled directly or indirectly to the bottom of the S6 segment. The second is that the S4 segment is in contact with the S6 segment within the transmembrane region, so that S4 movement is communicated directly to the S6 segment. Both of these allosteric coupling interactions may contribute to voltage-dependent gating and are not mutually exclusive.

An association between the S4–S5 linker and the bottom of the S6 segment has been proposed to explain the consequences of linker mutations on permeation properties in *Shaker* potassium channels (Slesinger et al., 1993). A similar association was proposed in studies of chimeric constructs of voltage-gated *Shaker* potassium channels with KcsA (Lu et al., 2001) and of HERG potassium channels (Tristani-Firouzi et al., 2002). If interaction between the S4–S5 linker and the bottom of S6 contributes to coupling, one would expect that mutations in the cytoplasmic end of S6 would affect charge movement, i.e., the Q–V relationship and/or kinetics of gating current. The S4 segment is also likely to be in direct contact with the S6 segment within the transmembrane region (Durell et al., 1998), allowing S4 conformation to be communicated directly to the S6 segments.

In a previous study, we substituted cysteines for each of eight consecutive residues below the bundle crossing of S6 segments in *Shaker* potassium channels and found that some cysteine mutants displayed a decrease in open probability and single channel conductance, based on nonstationary noise analysis. Examination of block by tetrabutylammonium

Submitted August 5, 2002, and accepted for publication September 20, 2002.

Address reprint requests to Dr. Richard Horn, Jefferson Medical College, Dept. of Physiology, Institute of Hyperexcitability, 1020 Locust Street, Philadelphia, PA 19107. Tel.: (215) 503-6725; Fax: (215) 503-2073; E-mail: Richard.Horn@TJU.edu.

0006-3495/03/01/295/11 $2.00

indicated that the change of single channel conductance was due to an increase in a local energy barrier to ion movement (Ding and Horn, 2002). Here we examine the effects of these and other S6 tail ($S6_T$) mutants on S4 movement assayed from gating currents, and on activation gate movement assayed from the voltage-dependence and kinetics of ionic currents. Perturbation of the $S6_T$ region has consequences on channel activation and especially on gating charge movement, suggesting a role in coupling.

MATERIALS AND METHODS

DNA clones and site-directed mutagenesis

The wild type (WT) background we use for mutations is *Shaker* H4 containing four modifications: deletion of residues 6–46 to remove N-type inactivation, T449V to inhibit C-type inactivation, and C301S and C308S to reduce sensitivity of the WT channel to cysteine modification (Holmgren et al., 1996). In order to increase the expression level, we introduced the Kozak consensus sequence (5′-GCCACCATGG; Kozak, 1991) before the coding region by site-directed mutagenesis. Based on this background, we constructed eight cysteine mutants (N482C, Y483C, F484C, Y485C, H486C, R487C, E488C, and T489C) and their nonconducting versions with the W434F mutation (Perozo et al., 1993) in the pore region. Mutagenesis was done with QuickChange™ Site-Directed Mutagenesis Kits from Stratagene (La Jolla, CA). All of the cDNA clones were sequenced to verify each mutation. We used a standard calcium phosphate method to transiently transfect tsA201 and HEK293 cells.

Electrophysiology

Standard whole cell patch-clamp recording methods (Ding and Horn, 2001) were used to record gating and ionic currents with an Axopatch 200B amplifier (Axon Instruments, Union City, CA). The patch pipette contained (mM): 105 CsF, 35 NaCl, 10 EGTA, 10 Hepes, pH 7.4. The bath contained (mM): 150 NaCl, 2 KCl, 1.5 $CaCl_2$, 1 $MgCl_2$, 10 Hepes, pH 7.4. All of the experiments were done at room temperature. Liquid junction potentials between the bath and the pipette solution were corrected. Electrode resistance was in the range of 1–2 M Ω. The voltage error due to series resistance was <3 mV after compensation. Data were collected between 8–12 min after the establishment of the whole cell configuration in order to avoid time-dependent changes of ionic tail currents and OFF gating currents. For experiments involving cysteine modification by intracellular methanethiosulfonate (MTS) reagents, aqueous stock solutions of 100 mM methanethiosulfonate-ethyltrimethylammonium (MTSET), methanethiosulfonate-ethylsulfonate (MTSES), methanethiosulfonate-2-aminoethyl (MTSEA), and an ethyl acetate stock solution of 100 mM benzophenone-4-carboxylamidocysteine methanethiosulfonate (BPMTS) were kept at 4°C and diluted to 1 mM in the pipette solution immediately before use. Complete modification was achieved within 10 min after the whole cell recording configuration was established. Whole cell and gating currents were low-pass filtered at 5–10 kHz and acquired with a DigiData 1200B digitizer using Clampex 8.0 (Axon Instruments) and sampled at 200 kHz. Capacitance and leakage currents were subtracted by the use of a $P/-8$ correction protocol from a –120-mV holding potential.

Data analysis

Data were analyzed using pCLAMP (Axon Instruments), ORIGIN 7.0 (OriginLab, Natick, MA), Fortran (Compaq, Houston, TX), and Maple (Waterloo Maple, Ontario, Canada). Throughout the paper, error bars represent the standard error of the mean.

G–V and Q–V relationship

For whole cell current recordings, the voltage-dependence of conductance (G) was estimated from tail currents at −60 mV. Except for the mutant F484C, the contamination of ionic tail currents by OFF gating current at this voltage is negligible. Voltage-dependence of charge (Q) movement was obtained by integration of OFF gating currents from nonconducting mutants at −120 mV. Both G–V and Q–V relations were fitted to the Boltzmann equation:

$$\mathrm{G(V)\ or\ Q(V)} = \frac{1}{1+\exp[-\mathrm{qF(V-V_{1/2})/RT}]}, \quad (1)$$

where $G(V)$ and $Q(V)$ are normalized conductance and gating charge, $V_{1/2}$ is the half activation or gating charge movement voltage, q is the charge, and RT/F is 25 mV at room temperature.

Analysis of periodicity

Fourier transform methods (Cornette et al., 1987; Li-Smerin et al., 2000a) were used to evaluate the periodicity of effects of mutations on gating currents. The Gibbs free energy (ΔG_0) was calculated as $\Delta G_0 = qFV_{1/2}$, with q and $V_{1/2}$ determined from Boltzmann fits to Q–V relationships. The change in ΔG_0 due to mutation at position j is $\Delta\Delta G_j = \Delta G_{0,j}^{mut} - \Delta G_0^{WT}$.

The discrete Fourier spectrum $P(\omega)$ of $\Delta\Delta G_j$ is defined in terms of angular frequency ω by

$$\mathrm{P}(\omega) = \mathrm{X}(\omega)^2 + \mathrm{Y}(\omega)^2, \quad (2)$$

where $X(\omega)$ and $Y(\omega)$ are

$$\mathrm{X}(\omega) = \sum_{j}^{n}[(\Delta\Delta G_j - \langle\Delta\Delta G_j\rangle)\sin(j\omega)], \quad \text{and}$$

$$\mathrm{Y}(\omega) = \sum_{j}^{n}[(\Delta\Delta G_j - \langle\Delta\Delta G_j\rangle)\cos(j\omega)],$$

n is number of residues, and $\langle\Delta\Delta G_j\rangle$ is the mean value of $\Delta\Delta G_j$. The α-periodicity index α-*PI* is the average value of $P(\omega)$ centered at 105°, relative to the average value of $P(\omega)$ in 0°∼180°:

$$\alpha\text{-PI} = \left[\frac{1}{30^\circ}\int_{90^\circ}^{120^\circ} \mathrm{P}(\omega)d\omega\right] \Big/ \left[\frac{1}{180^\circ}\int_{0^\circ}^{180^\circ} \mathrm{P}(\omega)d\omega\right]. \quad (3)$$

An ideal α-helical pattern is characterized by a value of α-*PI* greater than 2 (Cornette et al., 1987; Komiya et al., 1988).

To examine whether the ordered values of $\Delta\Delta G_j$ in our data could have produced α-*PI* values greater than 2 by chance, we used a randomization test (Lehmann, 1959; Patlak et al., 1986). Such tests have been shown to be most powerful for a large class of alternative hypotheses (Lehmann, 1959). The order of the $\Delta\Delta G_j$ values was scrambled (i.e., randomized) using a random number generator to produce 1000 artificial datasets, each of which was used to calculate a value of α-*PI*. Note that although there are only eight cysteine mutants, we only examine 1000 out of the 8! = 40,320 possible ordered data sets. The distribution of α-*PI* values for these randomized datasets was compared with the value obtained from the original unscrambled dataset. The original α-*PI* value was considered significant if it was greater than 95% of the values in the randomized datasets. These calculations were done by a Fortran program.

RESULTS

We examined eight residues (N482–T489) downstream from the activation gate of the S6 segment, referred to as the S6 tail or $S6_T$, to test for the role of this region in activation gating and charge movement. $S6_T$ residues were substituted

individually by cysteines in a *Shaker* construct with the cytoplasmic inactivation ball removed and the point mutation T449V that significantly reduces C-type inactivation. We used this construct as the WT background for our cysteine mutations. Exploiting the poorly permeant cation Cs^+ as a charge carrier rather than K^+, we were able to record ionic and gating current simultaneously (Ding and Horn, 2001; Horn et al., 2000; Olcese et al., 1997).

Ionic current

Fig. 1 shows whole cell currents in response to families of depolarizations for the wild type channel and each cysteine mutant. Cursory inspection of these currents reveals two notable properties. First, the kinetics of deactivating tail currents vary considerably for individual mutants, slowest for N482C and fastest for F484C[1]. Note that we measured these tail currents at a relatively depolarized voltage of −60 mV to avoid contamination by OFF gating currents, which have very small amplitudes except at more hyperpolarized voltages (e.g., Fig. 2). Second, the relative amplitudes of peak ionic and gating current at depolarized voltages differ among the mutants. At +60 mV, the peak ionic current is ~3.8 times larger than the peak gating current for wild type channels. By contrast, the peak gating current for the F484C mutant is ~3 times larger than the ionic current at +60 mV. The ionic current is also relatively small in the Y485C mutant. The relatively small ionic currents in these two mutants are probably due to reductions of open probability and/or single channel conductance (Ding and Horn, 2002). We previously reported that F484C had both a decreased single channel conductance and a low open probability, while Y485C had only a decreased single channel conductance.

Gating current

Next we examine the effects of $S6_T$ mutations on S4 movement, as reflected in gating currents. Fig. 2 shows the gating currents of each cysteine mutant rendered nonconducting by the W434F mutation (Perozo et al., 1993). The ON gating current of each mutant increased in peak amplitude and rate of decay with increased depolarization. The OFF gating current is fast and without obvious rising phase after a small depolarization, and except for the mutants

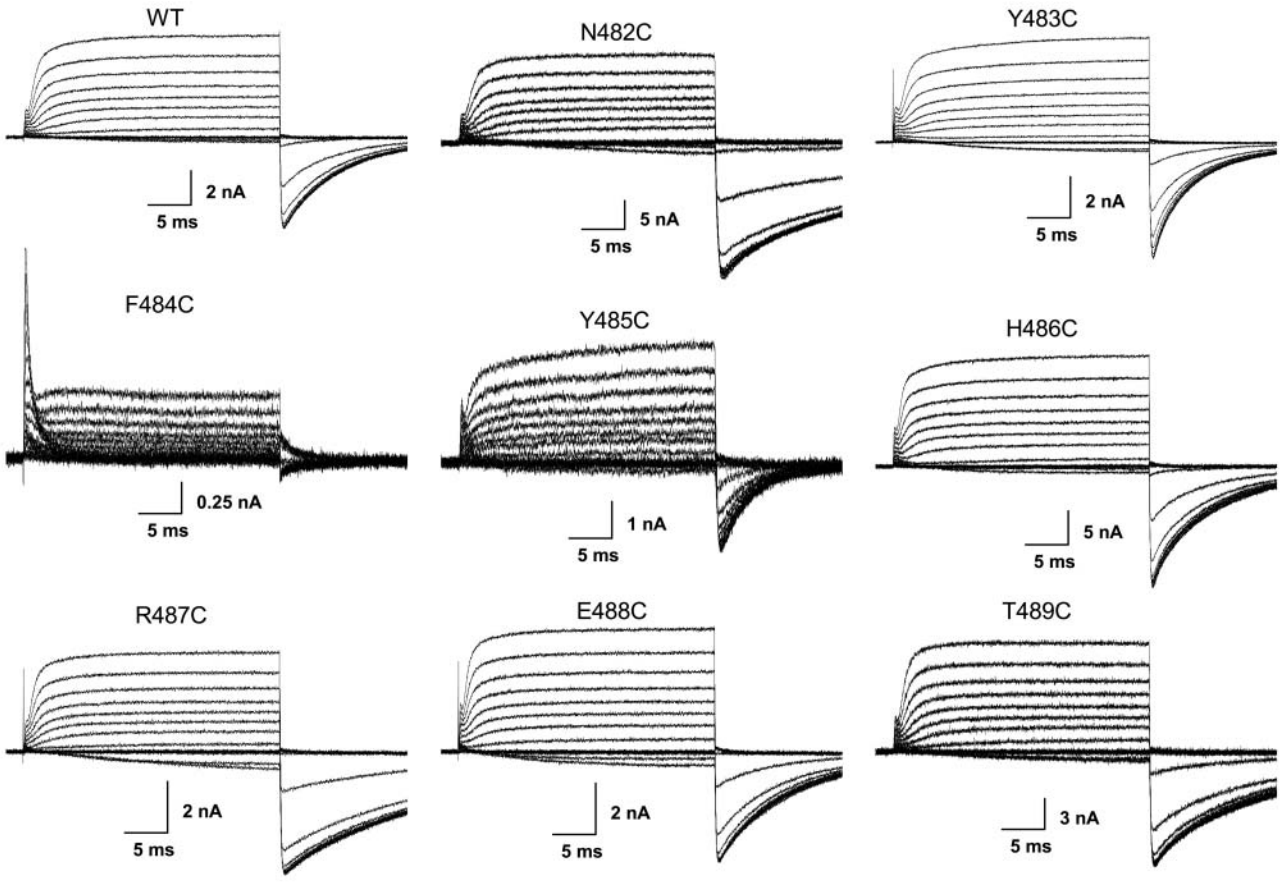

FIGURE 1 Ionic currents of WT and cysteine mutants. The currents were activated in response to depolarizing voltage steps from −100 mV to +40 mV in 5-mV steps and returned to −60 mV for measurement of deactivation kinetics. The holding potential was −120 mV. We plot here the currents at every 10-mV interval.

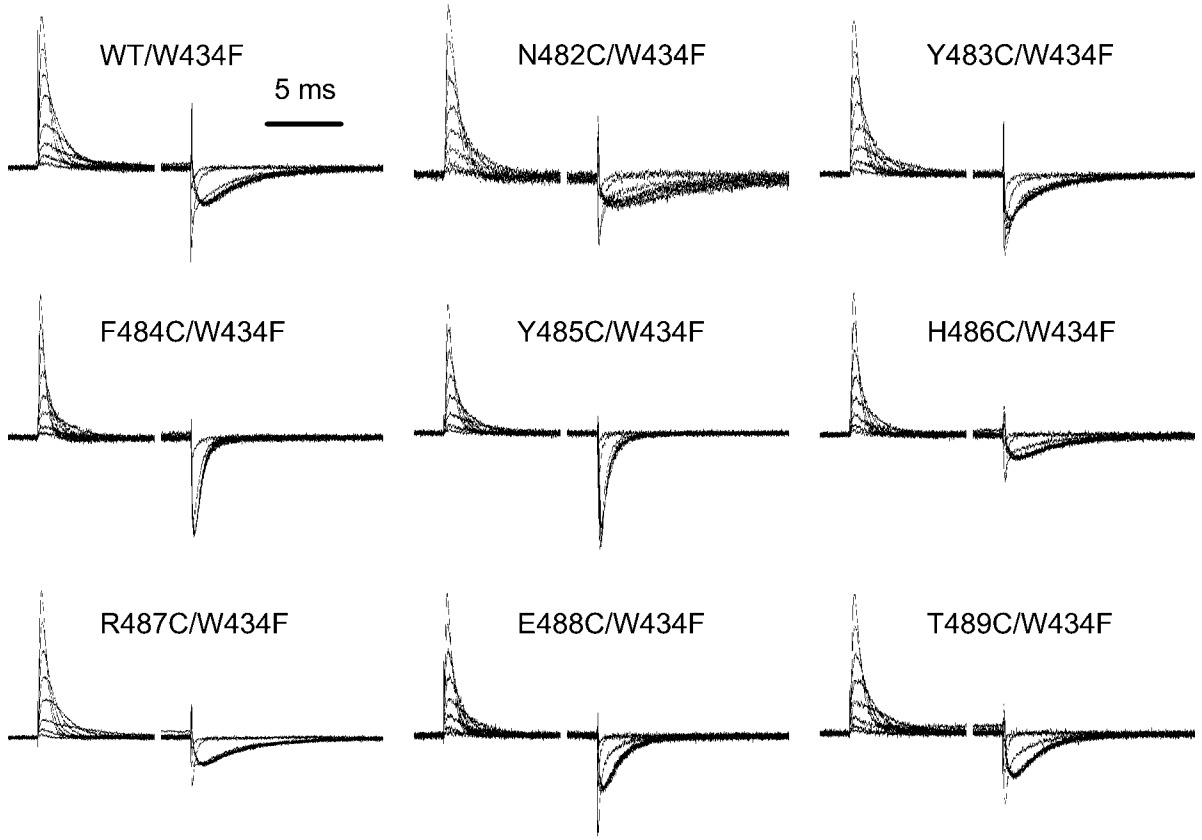

FIGURE 2 Gating currents of WT and cysteine mutants. The gating current families were recorded in response to 20-ms voltage steps from −100 to +60 mV in increments of 10 mV from a holding potential of −100 mV. The currents shown are from −80 mV in 20-mV increments to +60 mV.

F484C and Y485C, OFF gating currents exhibit a quick decay followed by a slower one after intermediate depolarizations. Following depolarizations to voltages larger than –30 mV, the OFF gating currents show a pronounced rising phase followed by a slow decay. The initial fast outward spike present in OFF gating currents, following a large depolarization in some cells, is likely due to contamination by nonlinear capacity currents during our capacitance correction procedure (Stühmer et al., 1991). The kinetics of ON gating currents in response to a series of depolarizations are rather comparable for all mutants, with decay time constants differing by less than a factor of two (Fig. 3 *A*). This suggests that early transitions along the activation pathway, primarily involving the independent movement of individual S4 segments (Bezanilla et al., 1994; Horn et al., 2000; Schoppa and Sigworth, 1998; Smith-Maxwell et al., 1998), are relatively insensitive to these mutations. By contrast, the OFF gating currents at –120 mV show a more pronounced mutation-dependent slow decay phase after depolarizations to voltages above about –30 mV (Fig. 2 and Fig. 3, *B* and *C*). N482C and F484C have the slowest and fastest OFF kinetics, respectively, the difference between them being larger than 10-fold. The channel constructs studied show a positive correlation between OFF gating current kinetics and decay kinetics of ionic tail currents at –120 mV (Fig. 3 *D*). This correlation is consistent with the coupling between voltage sensors and the activation gate for late transitions in the activation pathway, especially an open-to-closed transition. Although the correlation shown depends largely on the gating parameters from two mutants, N482C and Y485C, this relationship would be further strengthened if we could have included data from the F484C mutant, which has both the fastest deactivation kinetics and OFF gating current kinetics of all the constructs examined. However the ionic tail currents were too fast to be measured accurately.

These results confirm that mutations of $S6_T$ residues affect voltage sensor movement. Interestingly, the effects on steady-state charge movement are somewhat larger than those on the equilibrium between open and closed conformations of the activation gate (Fig. 4, Table 1). The range of $V_{0.5}$ shift of Q–V curves is ~20 mV among the mutants. The mutant F484C has the largest effect on the Q–V relationship, both on the slope (a 52% increase), and on the midpoint (an 11.4 mV hyperpolarizing shift compared to wild type channel). Another interesting characteristic of the F484C mutant is that it has a left-shifted Q–V curve (Fig. 4), but a right-shifted G–V curve (Fig. 2 in Ding and Horn,

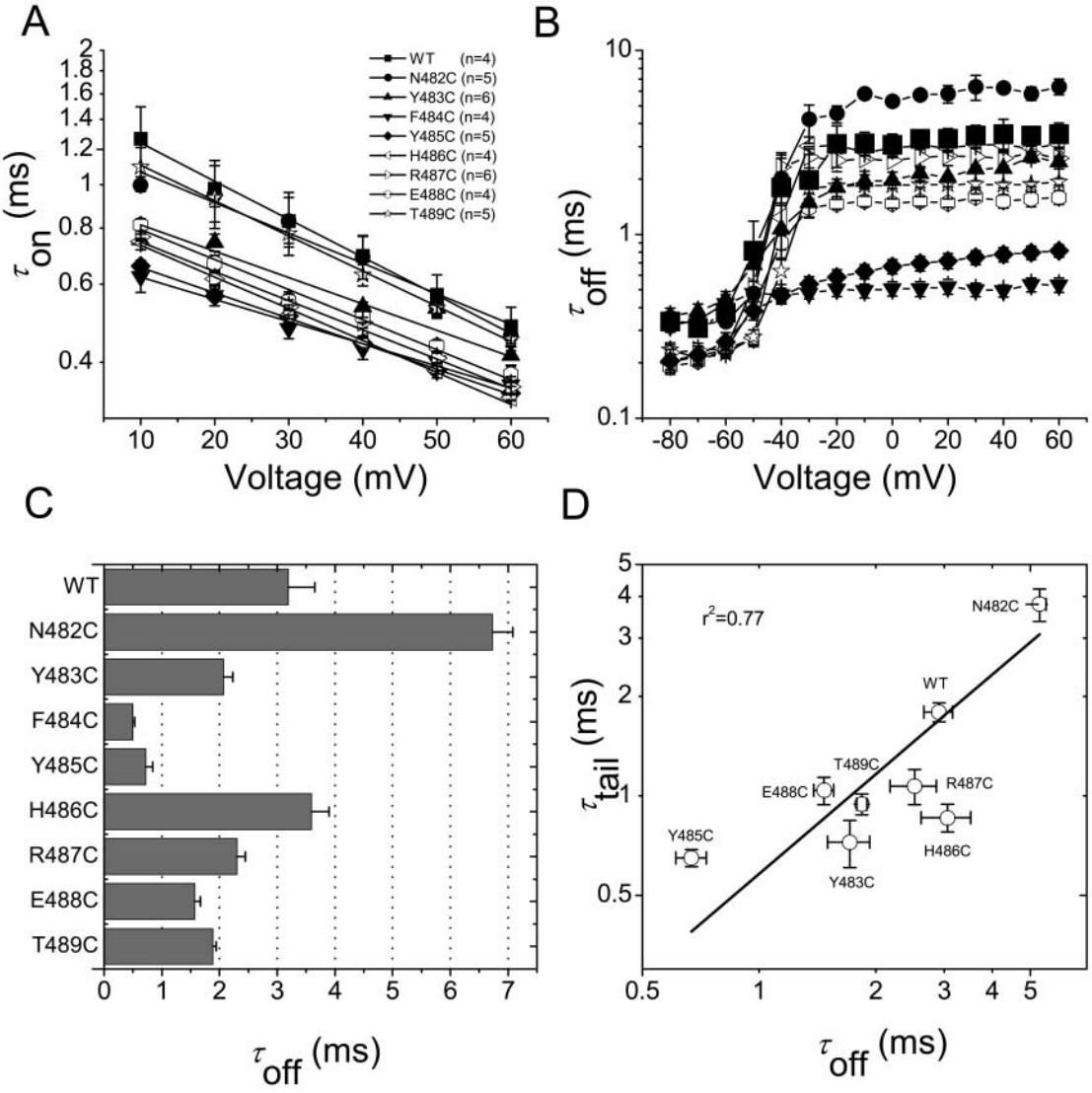

FIGURE 3 Time constants of ON and OFF gating currents. (*A*) Time constant of ON gating current decay in the voltage range between 10 and 60 mV vs. voltage. Single exponential relaxations from the peak were used. The plotted time constants were fitted with a single exponential function: $\tau_{on}(V) = \exp(-q_{on}V/kT)$. The partial charge values q_{on} were 0.49, 0.39, 0.29, 0.29, 0.33, 0.41, 0.38, 0.39, and $0.45e_o$ for WT, N482C, Y483C, F484C, Y485C, H486C, R487C, E488C, and T489C, respectively. (*B*) OFF gating current decay time constants at −120 mV plotted against the activating voltage. Following either very hyperpolarized or large depolarized voltage steps, the decay of OFF gating currents can generally be fitted by a single exponential function. As a rough approximation, we also fit the decay of OFF gating currents following intermediate voltage steps with a single exponential. (*C*) OFF time constants at −120 mV following a step to +40 mV. (*D*) Correlation between deactivation time constants of ionic currents (−120 mV) and gating current time constants (−120 mV) after depolarizations to +40 mV. Data from 3∼6 cells for each mutant. The correlation coefficient for these data was 0.77.

2001), suggesting that this mutation uncouples the movements of the voltage sensor and the activation gate.

Other substitutions at position 484 affect charge movement

Mutant F484C has the fastest OFF gating current decay and the largest Q–V shift among the cysteine mutants of $S6_T$. F484C also has a 31% reduction in single channel conductance (Ding and Horn, 2002). In order to test its sensitivity to structural perturbation, we substituted different amino acids at position 484 and measured Q–V and OFF gating current decay. Fig. 5 *A* shows the gating currents of WT and five mutant channels at position 484. The midpoints of Q–V relations vary over a range of ∼15 mV (Fig. 5 *B*). In general, residues with a bulky aromatic side chain have slower OFF gating currents after large depolarizations, compared to those with relatively small side chains (Fig. 5 *B*). This suggests that an aromatic side chain is important to maintain normal charge return from the open state. This conclusion is further validated by modifying F484C with methanethiosulfonate reagents. When F484C is modified by

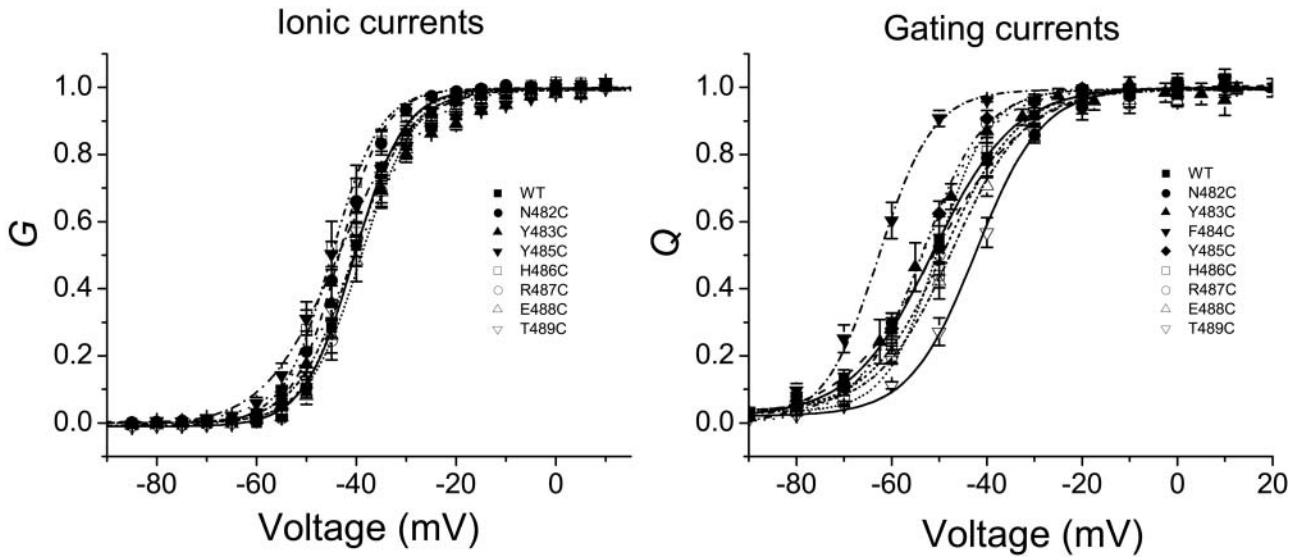

FIGURE 4 Normalized G–V and Q–V curves in conducting and nonconducting channels. The Q values were obtained from the numerical integration of OFF gating currents. The G values were obtained from the tail currents at −60 mV. Gating currents and ionic currents were measured under the same ionic condition. The smooth lines are fits to a Boltzmann function. The fitting parameters are summarized in Table 1.

BPMTS, which attaches a benzophenone moiety with two benzene rings to the cysteine, the OFF gating current decay becomes slow, similar to the WT, after large depolarizations (Fig. 5 *C*). However, when F484C is modified with the smaller hydrophilic reagents MTSEA, MTSET, and MTSES, there is little effect on the OFF gating current decay (Figs. 5 *C* and 6 *A*).

Fig. 6 *A* plots the decay time constants of OFF gating currents after depolarizations to +40 mV for all variants of residue 484. This time constant depends strongly on the aromaticity of the side chain (solid circles in Fig. 6 *B*) and shows no correlation with side chain molecular weight (Fig. 6 *B*) or side chain volume (data not shown). Our previous results showed that the maximum open probability of the cysteine mutant F484C is only 45% that of the WT (Ding and Horn, 2002), consistent with a destabilized open state. This could be a consequence of a faster open→closed rate, which reasonably would correlate with faster kinetics of OFF gating currents. The results of Fig. 6 show that constructs in which 484 residues have small non-aromatic side chains expedite closing rates.

Analysis of periodicity

Shifts of the Q–V relationships (Table 1) for successive cysteine mutants show a periodicity that may give some insight into the secondary structure of the $S6_T$ region. To

TABLE 1 Effects of Mutations on *Q–V* and *G–V* Relationships

	Q–V		*G–V*	
	$V_{0.5}$ (mV)	q (e_O)	$V_{0.5}$ (mV)	q (e_O)
WT	−51.3 ± 2.4;	2.9 ± 0.4 ($n = 4$)	−40.5 ± 0.8;	5.0 ± 0.1 ($n = 4$)
N482C	−51.0 ± 2.3;	2.5 ± 0.2 ($n = 7$)	−43.4 ± 1.6;	5.5 ± 0.2 ($n = 5$)
Y483C	−53.6 ± 1.9;	3.5 ± 0.2 ($n = 6$)	−41.6 ± 0.5;	3.5 ± 0.1 ($n = 5$)
F484C[1,2]	−62.7 ± 1.4;	4.4 ± 0.5 ($n = 4$)		
Y485C	−53.4 ± 1.0;	3.9 ± 0.1 ($n = 5$)	−44.0 ± 1.1;	3.4 ± 0.2 ($n = 4$)
H486C	−48.9 ± 1.3;	3.2 ± 0.1 ($n = 4$)	−45.0 ± 1.4;	5.2 ± 0.2 ($n = 5$)
R487C	−49.4 ± 1.1;	4.6 ± 0.3 ($n = 6$)	−40.4 ± 1.5;	5.1 ± 0.3 ($n = 4$)
E488C	−47.3 ± 1.5;	3.2 ± 0.2 ($n = 4$)	−39.0 ± 1.3;	4.7 ± 0.1 ($n = 4$)
T489C	−42.3 ± 1.3;	3.6 ± 0.2 ($n = 5$)	−40.7 ± 0.7;	4.5 ± 0.3 ($n = 4$)

Values from fits to single Boltzmann functions.

[1]G–V data were not obtained for F484C for Cs^+ currents in whole cell recording, because the tail currents did not allow an unambiguous measurement due to small amplitude and contamination by gating currents.

[2]In addition to having rapid kinetics, the ionic tail currents for F484C are small in amplitude. Although larger at more hyperpolarized voltages, the time course of deactivating ionic currents overlapped that of the OFF gating currents in this mutant at –120 mV (data not shown). Deactivation of ionic currents could not therefore be measured accurately under these ionic conditions.

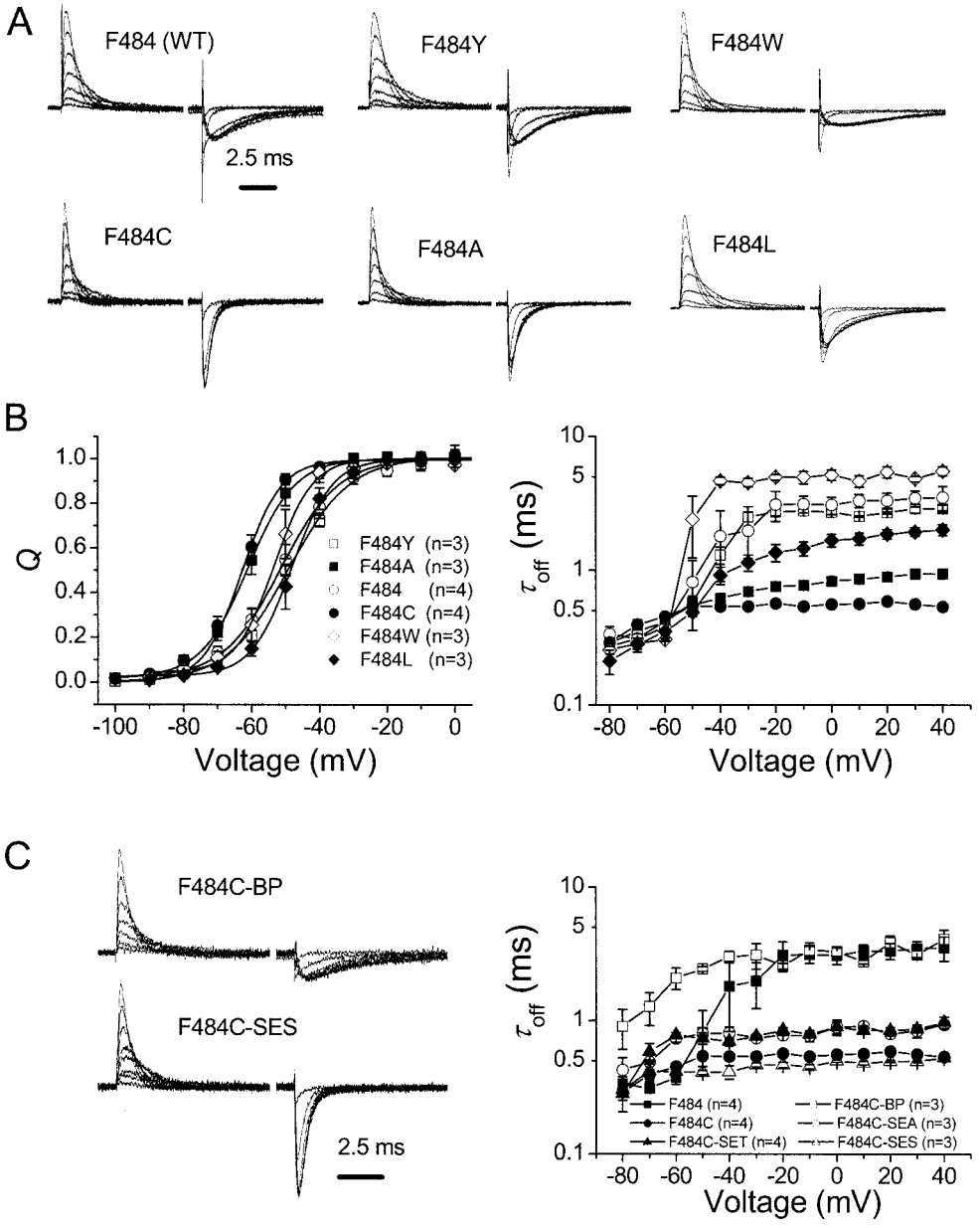

FIGURE 5 The effect of mutagenesis of residue 484 and MTS modification of F484C on the rate of gating charge return. (*A*) Gating currents of WT and mutants. The gating current families were recorded at the same condition as in Fig. 2. (*B, Left*) *Q–V* curves of WT and mutants. (*B, Right*) Decay time constants of OFF gating currents of WT and mutants at −120 mV as function of the activating voltage. (*C, Left*) Gating currents of F484C modified by BPMTS and MTSES. (*C, Right*) Decay time constants of OFF gating currents of WT and MTS-modified F484C at −120 mV as function of the activating voltage.

explore these features, we subjected the fitted parameters of these *Q–V* relationships to a Fourier analysis of periodicity (see Methods) after converting the data into free energy differences from wild type values (Fig. 7 *A*). Fig. 7 *B* shows the discrete power spectrum for the *Q–V* shifts which has a major peak centered at 108°. This spectrum is suggestive of an amphipathic α-helix, which is expected to produce a peak near 100°, the angle subtended by successive side chains in a canonical α-helix. The periodicity index, α-*PI*, is used to provide an objective criterion of helicity. α-*PI* values >2 are considered evidence of an α-helical structure (Cornette et al., 1987; Komiya et al., 1988). The spectrum in Fig. 7 *B* has an α-*PI* value of 2.41, suggesting that this short stretch of residues has an α-helical structure.

Although this α-*PI* value is >2, we were concerned that the apparent periodicity might be a chance occurrence due to the small number of residues (eight) in our study. To investigate this possibility we employed a nonparametric statistical procedure known as a randomization test (see Methods). We wanted to test whether the high α-*PI* values we obtained could have occurred by the chance ordering of the measured $\Delta\Delta G_j$ values for these cysteine mutants. We therefore created 1000 datasets, each of which contained the original eight $\Delta\Delta G_j$ values, but in randomized order. We calculated the α-*PI* values for each of these datasets and compared the distribution of α-*PI*s in the randomized datasets to that obtained from the original ordered dataset. The distribution is shown in Fig. 7 *C* with an arrow

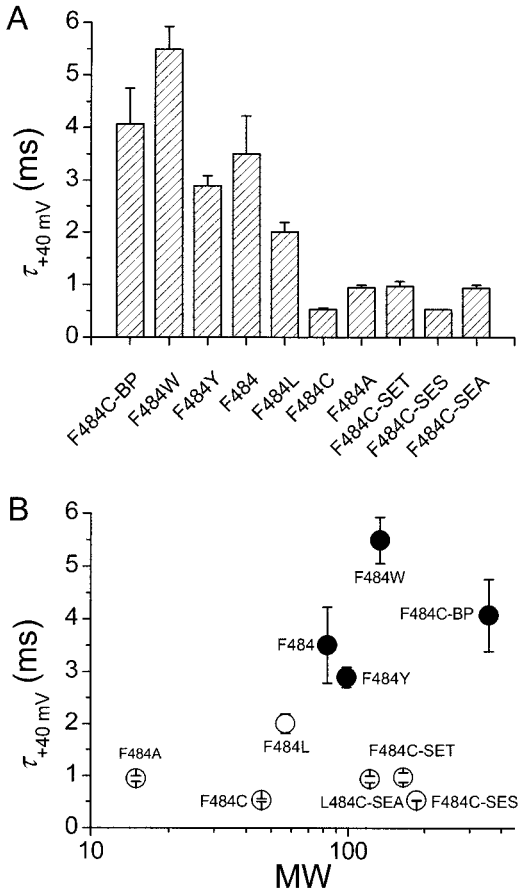

FIGURE 6 Aromatic side chains on residue 484 slow gating charge return. (*A*) OFF gating current decay time constants at −120 mV after an activating step to +40 mV of all variants of residue 484. (*B*) OFF gating current decay time constants plotted as function of molecular weight of the side chain.

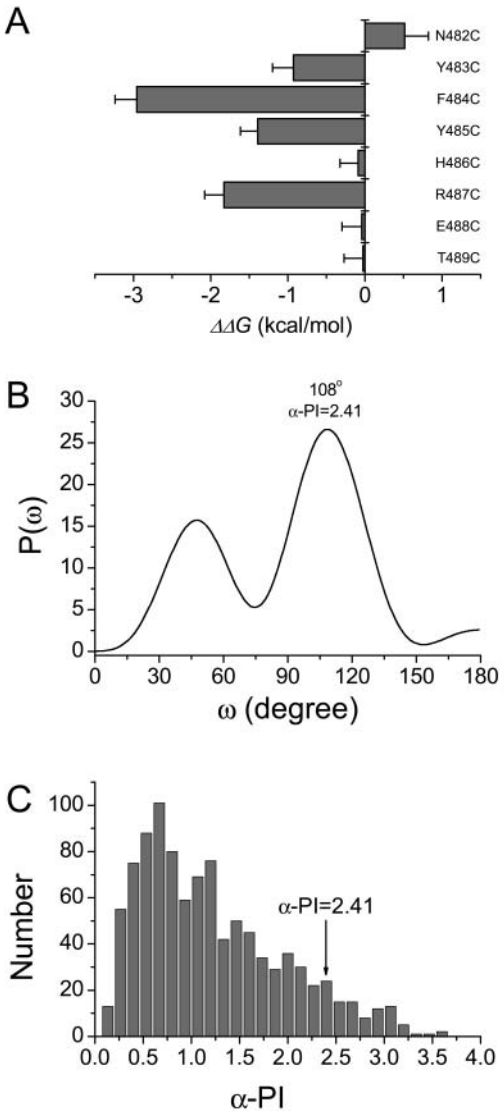

FIGURE 7 Periodicity analysis of effects of cysteine mutations. (*A*) $\Delta\Delta G_j$ values from *Q–V* curves. (*B*) Discrete Fourier spectrum derived from the $\Delta\Delta G_j$ values in *A*. (*C*) histogram of *α-PI* values for 1000 datasets in which the orders of $\Delta\Delta G_j$ values from original dataset that produced the above spectrum were randomized.

designating the original *α-PI* value. For the *Q–V* measurement, 72 of the 1000 *α-PI* values were greater than *α-PI* of the original dataset. Therefore, although the original *α-PI* values of the spectrum shown in Fig. 7 *B* is >2, this may have occurred by chance ($P \approx 0.072$). Therefore, the *α*-helicity of the $S6_T$ region remains unsettled.

DISCUSSION

We previously showed that mutations in the $S6_T$ region affect ion permeation and open channel block due to increases of a local energy barrier (Ding and Horn, 2002). Here we further report that the $S6_T$ region influences activation gating and charge movement. The main effects of $S6_T$ mutations are *Q–V* shifts and changes in the time constants of ionic tail currents and OFF gating currents. The positive correlation between these latter two kinetic parameters is consistent with the typically strong coupling between activation gating and charge movement (Sigg and Bezanilla, 1997; Sigworth, 1994). The residue that is most sensitive to cysteine substitution is F484. Our results suggest that an aromatic side chain at this position is critical for its normal contribution to gating. Finally, a spectral analysis of the effects of cysteine mutants shows evidence for *α*-helical periodicity, although a randomization test does not lead to a high level of confidence in this conclusion.

The two aromatic residues in $S6_T$, F484 and Y485, are highly conserved among K_V channels. Y485 is absolutely conserved, whereas F484 is only substituted by tyrosine or isoleucine (Liu et al., 1997). Cysteine mutations of F484 and Y485 cause: 1. an increase in the rate of deactivation of ionic currents, 2. an increase in the rate of charge return seen in

OFF gating currents, 3. a small, but significant, decrease in the time constant for ON gating currents, and 4. a hyperpolarizing shift of the Q–V curve for F484C. Many of these effects can be described as a partial uncoupling of the conformation of the voltage sensor from that of the activation gate due to the structural perturbation caused by mutagenesis. Our results suggest, for example, that normal voltage sensor movement is impeded by coupling to the activation gate. Therefore, uncoupling can allow more rapid kinetics of charge movement in many of the mutants. This is especially manifest in transitions near the open state in the activation pathway, accounting for larger effects on OFF than ON gating current. Partially disrupted coupling in these mutants is also suggested by decreases in $P_{o,max}$ (Ding and Horn, 2002) and by hyperpolarizing shifts of Q–V curves in some constructs, as if unloading $S6_T$ from the S4–S5 linker allows the S4 segment to carry its positive charge outward more easily when depolarized.

The $S6_T$ region is just downstream from the activation gate formed by the bundle crossing of the channel's four S6 segments. Allosteric effects on the kinetics of ionic tail currents are not, therefore, difficult to rationalize, because conformational changes in this region are likely to accompany the opening and closing of the activation gate. But how does the $S6_T$ region affect the S4 movement that underlies gating current? We consider three possibilities. The first possibility is that $S6_T$ mutations produce global disruptions of structure that affect all biophysical properties of the channel. This possibility cannot be eliminated, although the consequences of these mutations are generally rather mild on gating and have little effect on the selectivity of the pore (Ding and Horn, 2002). The second possibility is that the cytoplasmic $S6_T$ region has direct interaction with the S4–S5 linker, as proposed previously (Horn, 2000; Lu et al., 2001; Tristani-Firouzi et al., 2002). Therefore, mutations in $S6_T$ might affect S4 movement due to conformational coupling between these cytoplasmic regions. Finally, mutations of $S6_T$ might produce upstream allosteric consequences on the S6 segment in its transmembrane region, where it is likely to directly contact the S4 segment (Durell et al., 1998).

Circumstantial evidence provides support for the last two of the above three possibilities—either a cytoplasmic contact between $S6_T$ and the S4–S5 linker, or a transmembrane interaction between the S4 and S6 segments. For example, as in the $S6_T$ region, mutations in the S4–S5 linker affect permeation, activation gating, and charge movement (Isacoff et al., 1991; McCormack et al., 1991; Sanguinetti and Xu, 1999; Schoppa et al., 1992; Slesinger et al., 1993; Tristani-Firouzi et al., 2002); however, the relative magnitudes of effects on these gating processes differs between $S6_T$ and the S4–S5 linker. Our results using $S6_T$ mutations show somewhat larger effects on charge movement than on activation gating (Fig. 4), whereas mutations of some S4–S5 residues produce dramatic effects on activation (shifts of $>$70 mV of G–V curves) with only minor consequences on charge movement (Schoppa et al., 1992). Although the collected results could be explained by a direct interaction between these cytoplasmic regions, this hypothesis remains speculative. Two studies, however, show the possibility of electrostatic interactions between specific residues in these two regions, one examining sodium channels (Smith and Goldin, 1997), the other the HERG potassium channel (Tristani-Firouzi et al., 2002). Our periodicity analysis suggests that the $S6_T$ region might have an α-helical structure. The S4–S5 linker has also been proposed to have an α-helical secondary structure (Duclohier et al., 1997; Ohlenschläger et al., 2002). It is tempting, therefore, to speculate that $S6_T$ and the S4–S5 loop form a helix bundle with a critical role in coupling charge movement and activation gating, although direct evidence is lacking.

Other studies suggest that interactions between S4 and S6 segments occur in the transmembrane region. For example, tryptophan scanning mutagenesis of the S6 segment of *Shaker* produces effects on ionic currents that could be explained by an interaction of the backside of the S6 helix (directed away from the central axis of the pore) with the S4 segment (Li-Smerin et al., 2000b). Mutagenesis above the S6 bundle crossing also affects gating currents (Ding et al., 2002; Hackos et al., 2002). Some of these effects could be due to direct interactions between S4 and S6 segments.

A 'kink' or 'bend' in the S6 segment is likely to direct the bottom part of S6 outward toward the S4 segment (Del Camino et al., 2000; Del Camino and Yellen, 2001), especially when the channel is open (Jiang et al., 2002a; Jiang et al., 2002b). One motivation for the suggestion of a kink is the presence of a conserved Pro-X-Pro sequence near the bottom of the S6 segments of all K_V channels. However, other voltage-gated potassium channels lack the Pro-X-Pro sequence to serve as inflection points for the postulated kink in *Shaker*. For example, calcium-activated potassium channels that are also voltage-dependent have a single proline near the bottom of S6 (Pallanck and Ganetzky, 1994), whereas the S6 segment of HERG potassium channels has no prolines (Warmke and Ganetzky, 1994). Likewise, the voltage-dependent *Shaker*-KcsA chimera (Lu et al., 2001) lacks prolines in its S6 segments. The crystal structure of the open MthK potassium channel suggests the presence of another kink, centered on a glycine residue that is seven residues upstream of *Shaker*'s Pro-X-Pro sequence (Jiang et al., 2002a; Jiang et al., 2002b). This kink also directs the bottoms of the four S6 segments outward toward other transmembrane segments when the channel is open.

A pivotal role for the $S6_T$ region in the coupling of gate opening with an activating stimulus is suggested by our understanding of structurally related ion channels, specifically cyclic nucleotide gated (CNG) and eukaryotic calcium-activated potassium channels. In both of these types of channels, cytoplasmic agonists bind with the C-terminal extensions of the $S6_T$ regions of individual subunits, causing

opening of the activation gate. One can easily imagine that conformational changes induced by these binding events are communicated directly to the $S6_T$ regions and from there to the transmembrane S6 segments, as proposed for homologous regions of a bacterial potassium channel (Jiang et al., 2002b). Detailed studies of the S6 and $S6_T$ regions of eukaryotic calcium-activated potassium channels remain to be undertaken. However some information is available for CNG channels, where agonist binding appears to cause a rotation of both the S6 segments and the $S6_T$ regions, and a concomitant widening of the opening at the bundle crossing (Eaholtz and Zagotta, 2001; Johnson and Zagotta, 2001). By contrast with the model of del Camino et al. (2000) for *Shaker*, in which $S6_T$ regions diverge from the central axis of the pore, the four $S6_T$ regions of CNG channel subunits are postulated to converge below the bundle crossing (Johnson and Zagotta, 2001). This convergence is also proposed for the cytoplasmic extensions of the inner helices of KcsA channels (Cortes et al., 2001). Although an interaction between $S6_T$ and the bottom of the S4 segment makes teleological sense for a voltage-gated channel, there is no obvious reason for the $S6_T$ regions of CNG channels, which are not voltage-dependent, to be oriented toward the membrane where they might be able to interact with the S4–S5 linker.

The results of this and a previous study (Ding and Horn, 2002) reveal functional roles for the $S6_T$ region of *Shaker* potassium channels. Permeation, activation gating, and charge movement are all affected by $S6_T$ mutations. Future studies will elucidate whether this region plays an essential role in coupling these biophysical properties.

We thank Drs. Carol Deutsch and Manuel Covarrubias for insightful comments on an earlier version of the manuscript.

Supported by Grant AR41691 to R.H. from the National Institutes of Health.

REFERENCES

Bezanilla, F. 2000. The voltage sensor in voltage dependent ion channels. *Physiol. Rev.* 80:555–592.

Bezanilla, F., E. Perozo, and E. Stefani. 1994. Gating of *Shaker* K^+ channels. II. The components of gating currents and a model of channel activation. *Biophys. J.* 66:1011–1021.

Cornette, J. L., K. B. Cease, H. Margalit, J. L. Spouge, J. A. Berzofsky, and C. DeLisi. 1987. Hydrophobicity scales and computational techniques for detecting amphipathic structures in proteins. *J. Mol. Biol.* 195:659–685.

Cortes, D. M., L. G. Cuello, and E. Perozo. 2001. Molecular architecture of full-length *KcsA*—role of cytoplasmic domains in ion permeation and activation gating. *J. Gen. Physiol.* 117:165–180.

Del Camino, D., M. Holmgren, Y. Liu, and G. Yellen. 2000. Blocker protection in the pore of a voltage-gated K^+ channel and its structural implications. *Nature.* 403:321–325.

Del Camino, D., and G. Yellen. 2001. Tight steric closure at the intracellular activation gate of a voltage-gated K^+ channel. *Neuron.* 32:649–656.

Ding, S., and R. Horn. 2001. Slow photo-cross-linking kinetics of benzophenone-labeled voltage sensors of ion channels. *Biochemistry.* 40: 10707–10716.

Ding, S., and R. Horn. 2002. Tail end of the S6 segment: role in permeation in *Shaker* potassium channels. *J. Gen. Physiol.* 120:87–97.

Ding, S., T. P. Nguyen, and R. Horn. Molecular participants in voltage-dependent gating. *In* Epithelia, Pumps, Transporters and Ion Channels. F. Sepúlveda and F. Bezanilla, editors. Kluwer Academic/Plenum Press, New York. (In press).

Doyle, D. A., J. M. Cabral, R. A. Pfuetzner, A. L. Kuo, J. M. Gulbis, S. L. Cohen, B. T. Chait, and R. MacKinnon. 1998. The structure of the potassium channel: molecular basis of K^+ conduction and selectivity. *Science.* 280:69–77.

Duclohier, H., O. Helluin, P. Cosette, A. R. Schoofs, S. Bendahhou, and H. W. Wróblewski. 1997. Dissecting out the individual contributions of homologous segments to the voltage dependence and ion selectivity of the sodium channel with the peptide strategy. *Chemtracts Biochem. Mol. Biol.* 10:189–206.

Durell, S. R., Y. Hao, and H. R. Guy. 1998. Structural models of the transmembrane region of voltage-gated and other K^+ channels in open, closed, and inactivated conformations. *J. Struct. Biol.* 121:263–284.

Eaholtz, G., and W. N. Zagotta. 2001. Conformational changes in S6 coupled to the opening of cyclic nucleotide-gated channels. *Neuron.* 30:689–698.

Hackos, D. H., T. H. Chang, and K. J. Swartz. 2002. Scanning the intracellular S6 activation gate in the *Shaker* K^+ channel. *J. Gen. Physiol.* 119:521–531.

Holmgren, M., M. E. Jurman, and G. Yellen. 1996. N-type inactivation and the S4–S5 region of the *Shaker* K^+ channel. *J. Gen. Physiol.* 108: 195–206.

Holmgren, M., K. S. Shin, and G. Yellen. 1998. The activation gate of a voltage-gated K^+ channel can be trapped in the open state by an intersubunit metal bridge. *Neuron.* 21:617–621.

Horn, R. 2000. Conversation between voltage sensors and gates of ion channels. *Biochemistry.* 39:15653–15658.

Horn, R., S. Ding, and H. J. Gruber. 2000. Immobilizing the moving parts of voltage-gated ion channels. *J. Gen. Physiol.* 116:461–475.

Isacoff, E. Y., Y. N. Jan, and L. Y. Jan. 1991. Putative receptor for the cytoplasmic inactivation gate in the *Shaker* K^+ channel. *Nature.* 353:86–90.

Jiang, Y. X., A. Lee, J. Y. Chen, M. Cadene, B. T. Chait, and R. MacKinnon. 2002a. Crystal structure and mechanism of a calcium-gated potassium channel. *Nature.* 417:515–522.

Jiang, Y. X., A. Lee, J. Y. Chen, M. Cadene, B. T. Chait, and R. MacKinnon. 2002b. The open pore conformation of potassium channels. *Nature.* 417:523–526.

Johnson, J. P., Jr., and W. N. Zagotta. 2001. Rotational movement during cyclic nucleotide-gated channel opening. *Nature.* 412:917–921.

Komiya, H., T. O. Yeates, D. C. Rees, J. P. Allen, and G. Feher. 1988. Structure of the reaction center from *Rhodobacter sphaeroides* R-26 and 2.4.1: symmetry relations and sequence comparisons between different species. *Proc. Natl. Acad. Sci. USA.* 85:9012–9016.

Kozak, M. 1991. Structural features in eukaryotic mRNAs that modulate the initiation of translation. *J. Biol. Chem.* 266:19867–19870.

Lehmann, E. L. 1959. Testing Statistical Hypotheses. John Wiley & Sons, New York.

Li-Smerin, Y., D. H. Hackos, and K. J. Swartz. 2000a. α-Helical structural elements within the voltage-sensing domains of a K^+ channel. *J. Gen. Physiol.* 115:33–49.

Li-Smerin, Y. Y., D. H. Hackos, and K. J. Swartz. 2000b. A localized interaction surface for voltage-sensing domains on the pore domain of a K^+ channel. *Neuron.* 25:411–423.

Liu, Y., M. Holmgren, M. E. Jurman, and G. Yellen. 1997. Gated access to the pore of a voltage-dependent K^+ channel. *Neuron.* 19:175–184.

Lu, Z., A. M. Klem, and Y. Ramu. 2001. Ion conduction pore is conserved among potassium channels. *Nature.* 413:809–813.

McCormack, K., M. A. Tanouye, L. E. Iverson, J.-W. Lin, M. Ramaswami, T. McCormack, J. T. Campanelli, M. K. Mathew, and B. Rudy. 1991. A

role for hydrophobic residues in the voltage-dependent gating of *Shaker* K^+ channels. *Proc. Natl. Acad. Sci. USA*. 88:2931–2935.

Ohlenschläger, O., H. Hojo, R. Ramachandran, M. Görlach, and P. I. Haris. 2002. Three-dimensional structure of the S4–S5 segment of the *Shaker* potassium channel. *Biophys. J*. 82:2995–3002.

Olcese, R., R. Latorre, L. Toro, and F. Bezanilla. 1997. Correlation between charge movement and ionic current during slow inactivation in *Shaker* K^+ channels. *J. Gen. Physiol*. 110:579–589.

Pallanck, L., and B. Ganetzky. 1994. Cloning and characterization of human and mouse homologs of the *Drosophila* calcium-activated potassium channel gene, slowpoke. *Hum. Mol. Genet*. 3:1239–1243.

Patlak, J. B., M. Ortiz, and R. Horn. 1986. Opentime heterogeneity during bursting of sodium channels in frog skeletal muscle. *Biophys. J*. 49:773–777.

Perozo, E., R. MacKinnon, F. Bezanilla, and E. Stefani. 1993. Gating currents from a nonconducting mutant reveal open–closed conformations in *Shaker* K^+ channels. *Neuron*. 11:353–358.

Sanguinetti, M. C., and Q. P. Xu. 1999. Mutations of the S4–S5 linker alter activation properties of HERG potassium channels expressed in *Xenopus* oocytes. *J. Physiol*. 514:667–675.

Schoppa, N. E., K. McCormack, M. A. Tanouye, and F. J. Sigworth. 1992. The size of gating charge in wild-type and mutant *Shaker* potassium channels. *Science*. 255:1712–1715.

Schoppa, N. E., and F. J. Sigworth. 1998. Activation of *Shaker* potassium channels. III. An activation gating model for wild-type and V2 mutant channels. *J. Gen. Physiol*. 111:313–342.

Sigg, D., and F. Bezanilla. 1997. Total charge movement per channel—the relation between gating charge displacement and the voltage sensitivity of activation. *J. Gen. Physiol*. 109:27–39.

Sigworth, F. J. 1994. Voltage gating of ion channels. *Q. Rev. Biophys*. 27:1–40.

Slesinger, P. A., Y. N. Jan, and L. Y. Jan. 1993. The S4–S5 loop contributes to the ion-selective pore of potassium channels. *Neuron*. 11:739–749.

Smith-Maxwell, C. J., J. L. Ledwell, and R. W. Aldrich. 1998. Role of the S4 in cooperativity of voltage-dependent potassium channel activation. *J. Gen. Physiol*. 111:399–420.

Smith, M. R., and A. L. Goldin. 1997. Interaction between the sodium channel inactivation linker and domain III S4–S5. *Biophys. J*. 73:1885–1895.

Stühmer, W., F. Conti, M. Stocker, O. Pongs, and S. H. Heinemann. 1991. Gating currents of inactivating and non-inactivating potassium channels expressed in *Xenopus* oocytes. *Pflugers Archiv.-European J Physiol*. 418:423–429.

Tristani-Firouzi, M., J. Chen, and M. C. Sanguinetti. 2002. Interactions between S4–S5 linker and S6 transmembrane domain modulate gating of HERG K^+ channels. *J. Biol. Chem*. 277:18994–19000.

Warmke, J. W., and B. Ganetzky. 1994. A family of potassium channel genes related to Eag in *Drosophila* and mammals. *Proc. Natl. Acad. Sci. USA*. 91:3438–3442.

Yellen, G. 1998. The moving parts of voltage-gated ion channels. *Q. Rev. Biophys*. 31:239–295.